https://doi.org/10.5194/egusphere-2026-4754
Preprint. Discussion started: 10 August 2026

Aerosol microphysics from a polar-integrating nephelometer: shutter angles, information content and angular redundancy

Aleksander Pietruczuk[1], Ilya Bruchkouski[1], Artur Szkop[1], and Justyna Szymkowska[1]

[1]Institute of Geophysics, Polish Academy of Sciences, Warsaw, Poland

Correspondence: Aleksander Pietruczuk (alek@igf.edu.pl)

Abstract. A polar-integrating nephelometer enables measurements of aerosol light scattering at various shutter angles. There is currently no generally accepted methodology for selecting optimal angular configurations based on maximizing the instrument's sensitivity to specific microphysical particle parameters. A shutter angle of $\sim 60°$ is found to provide maximum discrimination between absorbing and non-absorbing aerosols, while small angles (between 0° and 20°) and maximum angle (90°) are preferable for distinguishing non-absorbing aerosol types. This conclusion is obtained by performing a comprehensive *derivative-based global sensitivity* (DGSM) analysis, *degrees of freedom for signal* (DFS) assessment, and variance-ratio analysis for aerosol type discrimination to determine optimal measurement conditions, quantify retrievable parameters, and establish the limits of applicability of nephelometer data. A forward model of the polar-integrating nephelometer is studied within the GRASP analytical framework. The analysis includes global sensitivity assessment, estimation of minimum detectable concentration changes, DFS analysis via singular value decomposition, and calculation of the variance-ratio metric for ranking shutter positions. The results demonstrate that maximum sensitivity is observed for fine-mode particles with radii of 113–439 nm (for concentration), 86–335 nm (for the real part of the refractive index), and 148–576 nm (for the imaginary part). To detect a 3% change in the signal, concentration changes of less than 1 $\mu m^3\,cm^{-3}$ are sufficient for particles with radii below 1 µm, whereas for particles in the 3–5 µm range, changes of 1–10 $\mu m^3\,cm^{-3}$ are required, and for particles larger than 5 µm, changes exceeding 10 $\mu m^3\,cm^{-3}$ are necessary, which makes the coarse mode non-retrievable. The DFS analysis indicates that for bimodal size distributions, the total number of degrees of freedom for signal is 3 for all investigated aerosol types. Based on the Fisher information matrix analysis, three retrievable parameter combinations are identified (in order of decreasing information content): total aerosol concentration, fine-to-coarse mode partitioning, and effective particle radius. The results show that the limited information content of polar-integrating nephelometer measurements is a direct consequence of the compact and smoothing nature of the scattering operator, which restricts the effective dimensionality of the measurement space despite the availability of multiple angular observations.

https://doi.org/10.5194/egusphere-2026-4754
Preprint. Discussion started: 10 August 2026

1 Introduction

Atmospheric aerosol particles interact with solar radiation by scattering and absorbing light and therefore exert a direct influence on the Earth's radiative balance (Michibata et al., 2025). Despite their importance, the associated climate effects remain subject to large uncertainties, mainly due to the strong spatial and temporal variability of aerosol properties and their short atmospheric lifetime (Regayre et al., 2026). Consequently, progress in understanding aerosol–radiation interactions relies critically on accurate, direct in situ observations of aerosol optical properties rather than on indirect estimates derived from remote sensing or model-based approaches.

Nephelometers are among the most widely used instruments for direct measurements of aerosol light scattering (Horvath and Kaller, 1993). They use light scattered by aerosol particles over defined angular ranges and wavelengths, allowing the determination of key optical properties, such as the aerosol scattering and hemispheric backscattering coefficients. Integrating nephelometers have the ability to quantify the overall amount of light scattered by aerosols in some angular range and represent the most established class of such instruments (Beuttell and Brewer, 1949). Classic examples include the three-wavelength TSI 3563, which has served as a reference instrument for several decades (Anderson et al., 1996; Anderson and Ogren, 1998), as well as modern commercial systems such as the Aurora 3000 (Chamberlain-Ward and Sharp, 2011; Müller et al., 2011). These instruments measure total and backscattered light at multiple wavelengths and form the backbone of long-term in situ aerosol monitoring programs.

Data from integrating nephelometers are routinely used to derive intensive optical properties, including the scattering Ångström exponent and the backscattering fraction (Massoli et al., 2009). Their operation is governed by harmonized calibration procedures, quality-control protocols, and traceability requirements, particularly within large observational infrastructures. In this context, integrating nephelometers play a central role within the Aerosol, Clouds and Trace Gases Research Infrastructure (ACTRIS), which provides standardized and long-term aerosol observations across Europe and beyond (Laj et al., 2024).

While integrating nephelometers deliver robust bulk optical properties, they do not resolve the angular dependence of aerosol scattering. Full polar or imaging nephelometers address this limitation by directly measuring the aerosol scattering phase function over a wide range of angles (Bazo et al., 2024). Such measurements yield access to more detailed information related to particle size, shape, and refractive index and are therefore essential for optical closure studies, validation of light-scattering theories, and the development of inversion algorithms linking optical observations to aerosol microphysical properties (Espinosa et al., 2017).

The Aurora 4000 nephelometer occupies an intermediate position between classical integrating and full polar nephelometer concepts. It combines three-wavelength integrating nephelometry with angle-resolved scattering measurements obtained by varying the backscattering shutter position, thereby sampling light scattered in multiple angular sectors (Chamberlain-Ward and Sharp, 2011). This approach extends conventional integrating nephelometer observations by adding partial angular information while maintaining the robustness, automation, and long-term stability required for continuous in situ monitoring, including applications within the ACTRIS framework (Laj et al., 2024).

https://doi.org/10.5194/egusphere-2026-4754
Preprint. Discussion started: 10 August 2026

Beyond the retrieval of standard optical coefficients, nephelometer measurements inherently contain information related to aerosol microphysical properties (Moallemi et al., 2022). Because light scattering is sensitive to particle concentration, size distribution, and complex refractive index, multi-wavelength and angularly resolved nephelometer data can be used to constrain aspects of aerosol microphysics, for example through relationships with concentration proxies or moments of the particle size distribution (Anderson and Ogren, 1998; Espinosa et al., 2017). Therefore, in this study we investigate forward-model simulations to estimate the upper limit of the information content provided by the polar-integrating nephelometer (Aurora 4000), and to identify the optimal measurement configuration for the subsequent retrieval of aerosol microphysical parameters.

The rest of the paper is structured as follows: first we employ the GRASP forward model (Sect. 2.5) which is based on the equations of electromagnetic field interaction with homogeneous spherical particles of given physical parameters assuming single-scattering approximation [Dubovik et al., 2011, 2014, 2021]. GRASP approach has been previously applied not only to remote-sensing observations but also to angularly resolved in situ measurements; in particular, Espinosa et al. [2017] successfully used GRASP to retrieve aerosol optical and microphysical properties from an imaging polar nephelometer, demonstrating its suitability for interpreting angle-dependent scattering observations. In our implementation, the GRASP forward model describes how light scattering by aerosol particles is integrated over the angular ranges defined by the Aurora 4000 geometry: the lower integration limit is controlled by the shutter position (variable between about 10° and 90° in 18 discrete steps of approximately 5°), while the upper limit is fixed at about 170°. In addition to these angularly resolved signals, the instrument also provides a total scattering signal integrated over the full angular range. All simulations are performed at three wavelengths, allowing wavelength-dependent scattering effects to be incorporated into the analysis.

Using this forward model, we perform a global sensitivity analysis (Sect. 3.2) based on Derivative-Based Global Sensitivity Measures (GDSM) [Sobol, 2001; Sobol and Kucherenko, 2009]. This step quantifies how variations in aerosol concentration, particle size distribution, and complex refractive index propagate into the measured scattering signal and identifies which parameter contributes most strongly to the model response.

Next we quantify the information content and amount of independent parameters for the angularly resolved measurements by applying singular value decomposition analysis (Sect. 3.4). Further, we assess the detectability of aerosol concentration changes by evaluating which perturbations in selected particle size intervals produce measurable variations in the nephelometer signal under typical measurement conditions (Sect. 3.3).

Finally, (Sect. 3.6) we analyse the angular dependence of the integrated scattering signal for different representative aerosol types. This allows us to identify shutter positions that provide complementary sensitivity to aerosol optical and microphysical properties, and to evaluate the aerosol-type dependence of angular redundancy.

https://doi.org/10.5194/egusphere-2026-4754
Preprint. Discussion started: 10 August 2026

2 Methods

2.1 Global Sensitivity Analysis and Derivative-Based Measures

Global Sensitivity Analysis (GSA) evaluates how variations in model input parameters propagate to the model output over the entire admissible parameter space. For a forward model output y as a function of input parameters $x_1, \ldots, x_n$:

$$y = f(\mathbf{x}) = f(x_1, \ldots, x_n), \tag{1}$$

GSA quantifies parameter importance independently of a specific perturbation direction.

The widely used variance-based sensitivity indices (Sobol, 2001) provide a complete measure of parameter influence, but their estimation typically requires a large number of forward-model evaluations. In the present study, the forward model is evaluated on a predefined multidimensional grid of aerosol parameters, which naturally enables the calculation of local sensitivities through numerical derivatives. Consequently, derivative-based global sensitivity measures (DGSM) are adopted (Sobol and Kucherenko, 2009; Iooss et al., 2010). DGSM exploit the availability of model derivatives and quantify the expected value of squared sensitivities over the parameter space,

$$\nu_i = \mathbb{E}\left[\left(\frac{\partial f(\mathbf{x})}{\partial x_i}\right)^2\right], \tag{2}$$

where E[] denotes the expected value and ν_i represents the i-th DGSM that quantifies the absolute contribution of a given parameter i with the remaining parameters kept fixed.

In the case of forward models that map a set of internal system parameters $x_1, \ldots, x_n$ to a vector of measurable output data $y_1, \ldots, y_m$, the Jacobian can be calculated directly

$$\mathbf{J}_{ij} = \frac{\partial y_j}{\partial x_i}, \tag{3}$$

and the DGSM can be reduced to an arithmetic mean of the squared Jacobian values,

$$\nu_i = \overline{\left(\frac{\partial y_j}{\partial x_i}\right)^2}, \tag{4}$$

where ν_i can show the relative strength of the i^{th} input parameter on the j^{th} output parameter of the forward model, but do not provide information about whether this influence is independent or redundant.

In this study, this is achieved by combining global sensitivity analysis, Fisher information diagnostics, and singular value decomposition of the Jacobian matrix. These approaches address complementary aspects of the forward-model problem. Global sensitivity measures quantify how strongly individual parameters affect the model output, whereas the degrees of freedom for signal (DFS) quantify how many *independent* combinations of parameters are supported by the measurements. Importantly, a parameter may exert strong influence on the measurement while remaining informationally redundant due to correlations with other parameters.

https://doi.org/10.5194/egusphere-2026-4754
Preprint. Discussion started: 10 August 2026

2.1.1 Fisher Information Matrix and Parameter Correlations

In order to distinguish between independent and redundant parameter influences in the forward model, the Fisher Information Matrix is introduced as a diagnostic tool. Global sensitivity measures identify parameters that affect the measurements, but do not indicate whether these effects can be separated from one another. The Fisher matrix addresses this limitation by quantifying parameter coupling in the observation space, thereby enabling identification of parameter degeneracies.

In this study, the Fisher Information Matrix is evaluated locally for representative aerosol states, such that the resulting parameter correlations reflect the sensitivity structure specific to a given aerosol type or typical size distribution.

The Fisher Information Matrix is defined as

$$\mathbf{F} = \mathbf{J}^{\mathrm{T}}\mathbf{J}, \tag{5}$$

and its spectrum can show the amount of independent input parameters. In the present analysis, the Fisher matrix is evaluated in an unweighted form, assuming equal and uncorrelated measurement uncertainties, such that the results reflect the intrinsic structure of the forward operator independent of specific measurement error model. This approach can be understood as quantification of the best case scenario where inversion specific uncertainties are small compared to the forward model's inherent limitations.

Here, the diagonal elements of the Fisher matrix correspond to the squared norm of the Jacobian columns and are therefore directly related to derivative-based sensitivity measures, while the off-diagonal elements describe overlap between parameter sensitivities. From (Hansen, 1998), the eigenvalues of the Fisher matrix are equal to the squared singular values of the Jacobian,

$$\lambda_i(\mathbf{F}) = \sigma_i^2. \tag{6}$$

The normalized correlation matrix,

$$\rho_{kl} = \frac{F_{kl}}{\sqrt{F_{kk}F_{ll}}}, \tag{7}$$

provides insight into parameter coupling. Values $|\rho_{kl}| \to 1$ indicate strong linear dependencies, implying that the corresponding parameters cannot be independently constrained for the given aerosol state. These correlations correspond directly to near-linear dependencies between columns of the Jacobian, which manifest as small singular values.

2.2 Information Content and Degrees of Freedom

The concept of degrees of freedom for the signal (DFS) was introduced by Rodgers (2000) to quantify the number of combinations of independent parameters that can be constrained with a measurement. In the classical formulation, DFS arises from the analysis of the retrieval problem and depends on both the forward model and the a priori error statistics. In the present study, no retrievals were performed. Instead, the analysis focuses on the intrinsic information content of the forward operator itself.

To this end, the forward model is locally linearized around a selected reference state $\mathbf{x}_0$, of input parameters.

$$\mathbf{y}(\mathbf{x_0}) \approx \mathbf{\Phi}(\mathbf{x}_0) + \mathbf{J}(\mathbf{x}_0)(\mathbf{x} - \mathbf{x}_0), \tag{8}$$

https://doi.org/10.5194/egusphere-2026-4754
Preprint. Discussion started: 10 August 2026

where $\mathbf{J}$ is the Jacobian matrix that describes the sensitivity of the measurements to the model parameters and $\Phi(\mathbf{x}_0)$ is a vector function of the forward model. This linearized representation shows that the mapping between parameter variations and measurement space is fully determined by the Jacobian. Consequently, the number of combinations of independent parameters that can be distinguished is limited by the number of independent directions in $\mathbf{J}$, i.e. $rank(\mathbf{J})$.

Under these conditions, the forward model specific $DFS_{forward}$ can be interpreted as an inherent property of the forward operator $\Phi(\mathbf{x}_0)$. This interpretation is consistent with the theory of ill-posed problems, where the singular value spectrum governs the amount of information recoverable from the data (Hansen, 1998). Consequently, input parameters associated with sufficiently large singular values are regarded as containing useful non-redundant information, while input variables corresponding to small singular values have negligible influence on $\mathbf{y}(\mathbf{x}_0)$.

The structure of the Jacobian can be analyzed using singular value decomposition ,

$$\mathbf{J} = \mathbf{U}\,\mathbf{\Sigma}\,\mathbf{V}^{\mathrm{T}}, \tag{9}$$

where $\mathbf{U}$ and $\mathbf{V}$ are orthogonal matrices, and $\mathbf{\Sigma}$ is a diagonal matrix containing the singular values σ_k.

Large singular values correspond to parameter combinations that produce distinct and measurable effects, while small singular values indicate directions that are weakly expressed or redundant. The effective number of degrees of freedom for signal is therefore determined by the number of significant singular values of the Jacobian, which can be expressed as

$$\mathrm{DFS}_{\mathrm{forward}} = \#\{\sigma_k > \varepsilon\,\sigma_1\}, \tag{10}$$

where ε is a threshold parameter defining the minimum relative magnitude of singular values retained in the analysis. Here, $\#\{\cdot\}$ denotes the number of elements satisfying this condition. In practice, ε reflects the sensitivity of the measurement system and the distinction between information-bearing and negligible components.

This provides the necessary link between parameter sensitivity and the effective number of independent information channels revealed by the singular value decomposition of the Jacobian.

By linking parameter sensitivity and the effective number of independent information channels revealed by the singular value decomposition of the Jacobian, this formulation provides a forward-model equivalent of the DFS concept of Rodgers (2000), while isolating the intrinsic information content of the measurement system from the influence of error models and inversion assumptions.

2.3 Forward Operator Structure and Rank Limitation

The principle of integrating nephelometer measurements imposes a fundamental limitation on the information that can be extracted from the data. Each observation $\mathbf{S}(\theta)$ does not correspond to a local value of the scattering function $K(\theta)$, but rather to its integral over a range of angles,

$$S(\theta) = C \int_{\theta}^{\theta_{\max}} K(\theta')\,\mathrm{d}\theta', \tag{11}$$

https://doi.org/10.5194/egusphere-2026-4754
Preprint. Discussion started: 10 August 2026

where θ is the position of the shutter, $\theta_{\max}$ is the maximum scattering angle observed by the detector, and C is a calibration constant.

As a consequence, measurements taken at different shutter angles represent different realizations of the same underlying quantity, rather than independent observations. This structure propagates directly to the Jacobian matrix given by

$$J_{ij} = C \int_{\theta_j}^{\theta_{\max}} \frac{\partial K(\theta', \mathbf{x})}{\partial x_i} \, \mathrm{d}\theta', \tag{12}$$

which shows that each row of the Jacobian is an integral of the same scattering function with respect to the parameters, differing only by the lower integration limit. Consecutive measurements do not provide entirely new information, but contain partially overlapping contributions of the same signal. A measurement at a larger angle can be interpreted as a reduced version of a measurement at a smaller angle. This leads to strong correlations between observations.

From the perspective of the forward model, varying the measurement angle does not introduce new independent ways in which parameters affect the signal. Instead, it only changes the portion of the angular domain over which the same physical process is observed. The number of genuinely independent information channels is therefore limited by the structure of the measurement operator. In this context, the singular value spectrum of the Jacobian is expected to decay rapidly, indicating that only a limited number of independent information directions can be supported by the measurements. Consequently, increasing the number of angular observations may not lead to a proportional increase in the degrees of freedom for the signal (DFS), which are instead governed by the intrinsic smoothing properties of the forward operator. This behavior is consistent with the properties of Fredholm operators of the first kind, which act as smoothing operators and reduce the effective dimensionality of the signal space (Kress, 1999; Engl et al., 1996). Such operators are known to produce ill-posed problems characterized by rapidly decaying singular values (Hansen, 1998).

This interpretation provides a plausible physical explanation for the limited number of degrees of freedom for signal (DFS) in nephelometer measurements and suggests that only a small number of independent aerosol parameter combinations can be robustly constrained, even in the presence of dense angular sampling. The extent to which this theoretical limitation manifests in practice is examined in the following sections.

2.4 Angular discrimination metric

To investigate how the discriminatory power of nephelometer measurements depends on scattering angle, we define a variance-ratio metric that quantifies the separability of aerosol types. For each aerosol type, multiple forward model outputs are generated by varying the median radius r_m and geometric standard deviation σ_g. Each aerosol class is additionally characterized by a constant representative complex refractive index (n,k). The resulting nephelometer signals are normalized by the total-scattering measurement,

$$S_N(\theta) = \frac{S(\theta)}{S(\theta_0)}, \tag{13}$$

https://doi.org/10.5194/egusphere-2026-4754
Preprint. Discussion started: 10 August 2026

where θ_0 corresponds to the smallest shutter position, outside of the field of view of the detector.

To quantify the ability of a given shutter position and wavelength to discriminate between aerosol classes, we define the variance-ratio metric (i.e. discrimination metric)

$$D(\theta) = \frac{\mathrm{Var_{between}}}{\mathrm{Var_{within}}}, \tag{14}$$

where

$$\mathrm{Var_{between}} = \mathrm{Var}\left(\overline{S_N(\theta,\lambda)}\right) \tag{15}$$

is the variance of the signals averaged over all configurations of r_m and σ_g within a class $\overline{S_N(\theta,\lambda)}$ and

$$\mathrm{Var_{within}} = \overline{\mathrm{Var}(S_N(\theta,\lambda))} \tag{16}$$

denotes the mean variance of the signals within individual aerosol types.

Large values of $D(\theta,\lambda)$ indicate that different aerosol classes produce clearly distinguishable signals compared with their internal variability. In contrast, small values indicate poor class separation. This metric is closely related to the concept of Fisher discrimination, as it measures the ratio of inter-class variability to intra-class variability. Angular regions with large values of $D(\theta,\lambda)$ are therefore expected to provide enhanced discrimination between aerosol classes and may contribute more strongly to the independent information content of the measurements.

2.5 GRASP as a forward–modeling framework

GRASP (Generalized Retrieval of Aerosol and Surface Properties) is an open-source physically-based modeling and inversion framework designed for the analysis of aerosol and surface radiative properties (Dubovik et al., 2014, 2021). The framework is built upon a statistically optimized multi-term inversion approach, originally introduced by Dubovik et al. (2011), which combines measurement fitting with additional constraints and a priori information in a unified formulation. Its modular structure separates the forward radiative transfer model from the inversion engine, allowing a consistent physical description to be applied across different observation types.

In this study, the open-source version of the Generalized Retrieval of Atmosphere and Surface Properties (GRASP-OPEN version 1.1.6) is used exclusively as a forward–modeling tool. The model simulates angular scattering properties of aerosols as a function of particle size distribution, complex refractive index, and wavelength. Subsequently, it calculates the nephelometer signal by integrating the simulated phase function over angular ranges corresponding to the instrument geometry. This approach provides a direct and transparent mapping between aerosol microphysical properties and the measured signal, without introducing additional assumptions associated with inversion algorithms. As a result, the analysis focuses solely on the sensitivity and information content of the forward operator.

GRASP has been successfully applied across a wide range of observing systems, including polar nephelometers, lidar measurements, sun-photometers, satellite remote sensing, and their arbitrary combinations (e.g., Lopatin et al., 2013; Lopatin et al., 2021; Dubovik et al., 2014; Dubovik et al., 2021; Espinosa et al., 2017), demonstrating its capability to provide a consistent

https://doi.org/10.5194/egusphere-2026-4754
Preprint. Discussion started: 10 August 2026

Table 1. Parameterization of aerosol microphysical properties used in the forward model simulations.

Parameter	Discretization	Range
Aerosol size distribution	22 triangular bins (geometric spacing)	0.05–15.0 µm
Real part of refractive index	22 values (linear spacing)	1.29–1.69
Imaginary part of refractive index	15 values (geometric spacing)	5.0×10^{-4}–5.0×10^{-1}

physical description of aerosol optical properties across different measurement geometries. The flexibility of GRASP (OPEN) allows the level of aerosol parameterization to be adapted to the information content of the measurements, ensuring internal consistency between the forward model and the observational constraints.

3 Results

3.1 Forward Model Configuration and Simulation Setup

The fololowing results are based on a forward model of an integrating nephelometer configured to represent the measurement principle of the Aurora 4000 polar nephelometer. The aerosol population is parameterized using a discrete size distribution consisting of 22 triangular size bins, which corresponds to the standard GRASP configuration (Dubovik and King (2000),Dubovik et al. (2006)). The bin radii are spaced geometrically over the particle size range relevant for atmospheric aerosols. In addition to the size distribution, the complex refractive index of the aerosol is treated as a model parameter, particle sphericity was fixed at 0.99. The real part of the refractive index is sampled using a linear spacing, while the imaginary part is sampled using a geometric spacing in order to capture the broad dynamic range of aerosol absorption properties. The full aerosol parameterization employed in the forward simulations is summarized in Table 1.

Forward simulations of the nephelometer signal are performed at three wavelengths, namely 450, 525, and 635 nm, corresponding to the operational wavelengths of the Aurora 4000 instrument. For each wavelength, angularly integrated scattering signals are computed for shutter positions ranging from $0°$ to $90°$, with $5°$ step, while the full integration limit is achieved at $170°$ in all cases, as determined by the instrument geometry.

It should be noted that, for the actual Aurora 4000 nephelometer, physically realizable shutter positions correspond to angles of approximately $10°$ and larger. Furthermore, even the measurement of the total scattering coefficient does not represent integration from $0°$, but rather from a lower angular limit of approximately 7–$8°$ up to $170°$. These limitations (Müller et al. (2011)) arise from the optical geometry and truncation characteristics of the instrument. In the forward model, simulations including shutter positions below $10°$ are employed for sensitivity assessment and methodological completeness, while interpretations related to real measurements account for the practical angular constraints of the instrument.

The simulated angularly integrated scattering signals generated using this forward model constitute the dataset used in all subsequent analyses, including global sensitivity assessment, detectability of concentration changes, degrees of freedom for signal evaluation, and optimization of angular sampling.

https://doi.org/10.5194/egusphere-2026-4754
Preprint. Discussion started: 10 August 2026

3.2 Global sensitivity

Derivative–based global sensitivity measures (DGSM) valuse defined by Eq. 2 as partial derivatives of simulated signal with respect to the aerosol size-distribution bin concentrations, the real part of the refractive index n, and the imaginary part of the refractive index k.

In case of bin concentration

$$\nu_{C_i}(\theta) = \mathbb{E}\left[\left(\frac{\partial P_{\text{int}}(\theta)}{\partial c_i}\right)^2\right] = \mathbb{E}\big[\Phi_i(\theta)^2\big] \tag{17}$$

as

$$P_{\text{int}}(\theta) = \sum_{i=1}^{K} c_i\,\Phi_i(\theta) \tag{18}$$

where, $P_{\text{int}}(\theta)$ denotes the angularly integrated scattering signal measured at the shutter position θ, c_i represents the particle concentration in the i-th size bin, which is centered around particle radius r_i, $\Phi_i(\theta)$ denotes the contribution of the i-th aerosol size bin to the integrated scattering phase function at the shutter position θ.

Figure 1 shows $\nu_{C_i}(\theta)$ DGSM in color scale as a function of shutter and bin positions, right panel shows DGSM normalized to maximum value of each shutter position to emphasize variability related to bin position. In analog, Figures 2 and 3 present $\nu_n(\theta)$ and $\nu_k(\theta)$ DGSMs calculated numerically, respectively. The preliminary analysis indicates that the algorithm exhibits the highest sensitivity to aerosol size bins with diameters comparable to the wavelengths measured by the nephelometer. For perturbations in bin concentration, the strongest sensitivity is observed for particle radii in the range from approximately 113 to 439 nm (i.e. diameters of 226 to 878 nm). The sensitivity range is slightly shifted toward smaller particles for variations in the real part of the refractive index, corresponding to radii between about 86 and 335 nm (i.e. diameters of 172 to 670 nm). In contrast, sensitivity to changes in the imaginary part of the refractive index is shifted toward larger particles, with the dominant contribution arising from radii in the range of approximately 148 to 576 nm (i.e. diameters of 296 to 1152 nm). Moreover, the largest sensitivity is observed for small positions of the shutter.

This result is not unexpected and follows directly from scattering theory. The strongest scattering response and the largest variability in scattering are expected for particles with sizes comparable to the wavelengths of the incident light measured by the nephelometer. In this size regime, small changes in particle properties lead to the largest relative changes in the scattering signal. In addition, the sensitivity is highest for small shutter positions, which correspond to measurements that include, through angular integration, scattering contributions from all larger shutter positions. As a consequence, signals measured at small shutter angles accumulate scattering over the widest angular range, making them particularly more sensitive.

An analysis of the variability of GDSM values reveals pronounced differences across shutter angle ranges. In particular, enhanced variability is observed for intermediate shutter positions between approximately 40 and 60 degrees, as well as for large shutter positions exceeding about 80 degrees. This behavior suggests that these angular ranges may be useful for discriminating between different aerosol types characterized by distinct size distributions. The increased variability indicates a stronger sensitivity of the normalized signal to changes in aerosol properties, which is advantageous for aerosol type differentiation.

https://doi.org/10.5194/egusphere-2026-4754
Preprint. Discussion started: 10 August 2026

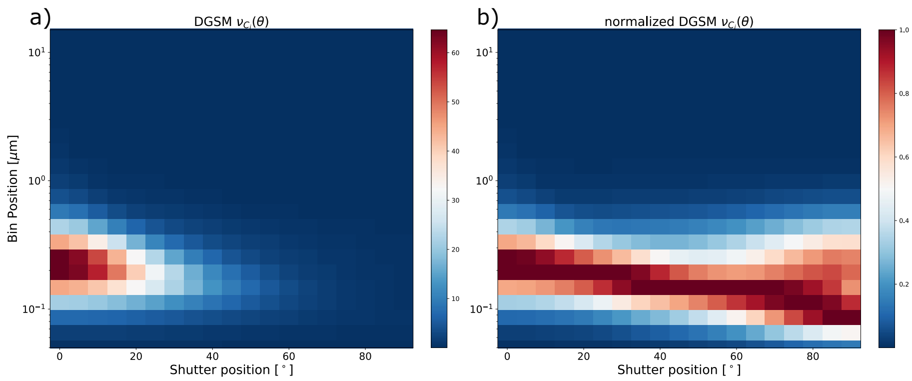

Figure 1. $\nu_{C_i}(\theta)$ DGSM as function fo shutter and bin positions.

However, this sensitivity is expected to be dominated primarily by the fine-mode aerosol fraction, as the GDSMs for large particles remain very small. Consequently, while these angular ranges carry discriminative information, their effectiveness is likely limited to variations in fine-mode aerosol characteristics rather than coarse-mode contributions.

The GDSM analysis of the complex refractive index reveals distinct behaviors for its real and imaginary components. Sensitivity to the real part is primarily controlled by shutter position and remains nearly independent of its magnitude, particularly for small shutter angles. A higher relative variability appears at larger shutter positions, indicating enhanced sensitivity for strongly scattering aerosols. In contrast, the imaginary part shows strong sensitivity for absorbing aerosols that decreases systematically with increasing shutter position. This behavior indicates that measurements at small shutter angles are especially sensitive to aerosol absorption, while the model sensitivity, dependent on normalized DGSM values, show highest values for radii between 100 nm and 300 nm, regardless of the shutter position.

3.3 Response of the Integrated Scattering Signal to Single–Bin Concentration Changes

The previous analysis indicates that the highest sensitivity of the integrated nephelometer signal is associated with aerosol size bins corresponding to the fine mode. This leads to the question of which particle concentrations, or more precisely which changes in the concentration of a given size bin, produce measurable variations in the nephelometer signal. To address this issue, a relative measurement sensitivity of the nephelometer of 3 % is assumed, corresponding to a detectable signal change of

$$0.03\,P_{\text{int}}(\theta). \tag{19}$$

For small perturbations, the resulting change in the integrated scattering signal can be approximated as

$$0.03\,P_{\text{int}}(\theta) \;\approx\; \Phi_i(\theta)\,\Delta c_i(\theta), \tag{20}$$

where $\Phi_i(\theta)$ denotes the contribution of the i-th size bin to the integrated scattering signal at shutter position θ, and $\Delta c_i(\theta)$ represents the corresponding change in the bin concentration.

https://doi.org/10.5194/egusphere-2026-4754
Preprint. Discussion started: 10 August 2026

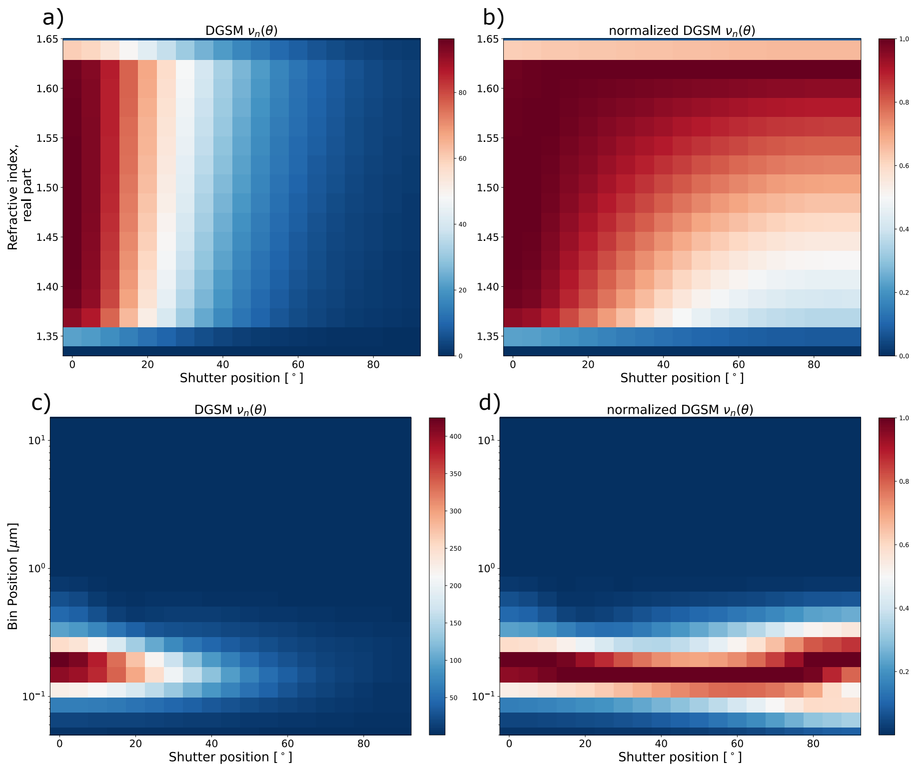

Figure 2. (a) $\nu_n(\theta)$ DGSM as a function of shutter and bin positions. (b) $\nu_n(\theta)$ as a function of the real part of the refractive index and bin position.

From this relation, the minimum detectable concentration change for the i-th size bin can be expressed as

$$\Delta c_i^{\min}(\theta) = \frac{0.03\, P_{\text{int}}(\theta)}{|\Phi_i(\theta)|}. \tag{21}$$

In addition to the previously computed values of $\Phi_i(\theta)$, this analysis requires a representative nephelometer signal. For this purpose, the median integrated scattering signal measured at the Racibórz observatory was used as a realistic reference. The analysis was carried out for both predominantly scattering aerosols (sulfate) and strongly absorbing fine aerosols, as defined in Table 3. This approach provides a quantitative estimate of the concentration changes required for detectability under typical atmospheric and instrumental conditions.

Figure 4 shows the aerosol concentration changes required to produce a 3 % variation in the integrated nephelometer signal. Concentration changes are expressed in $\mu\text{m}^3\,\text{cm}^{-3}$, which correspond directly to $\mu\text{g}\,\text{m}^{-3}$ assuming a particle density of 1 $\text{g}\,\text{cm}^{-3}$. The dashed and solid lines indicate concentration change thresholds of 1 and 10 $\mu\text{m}^3\,\text{cm}^{-3}$, respectively. The upper panel corresponds to a non-absorbing aerosol, while the lower panel shows results for an absorbing aerosol.

For submicron aerosol particles, with radii below approximately 1 μm, concentration changes smaller than 1 $\mu\text{m}^3\,\text{cm}^{-3}$ are sufficient to produce measurable variations in the nephelometer signal. This indicates a high sensitivity of the instrument

https://doi.org/10.5194/egusphere-2026-4754
Preprint. Discussion started: 10 August 2026

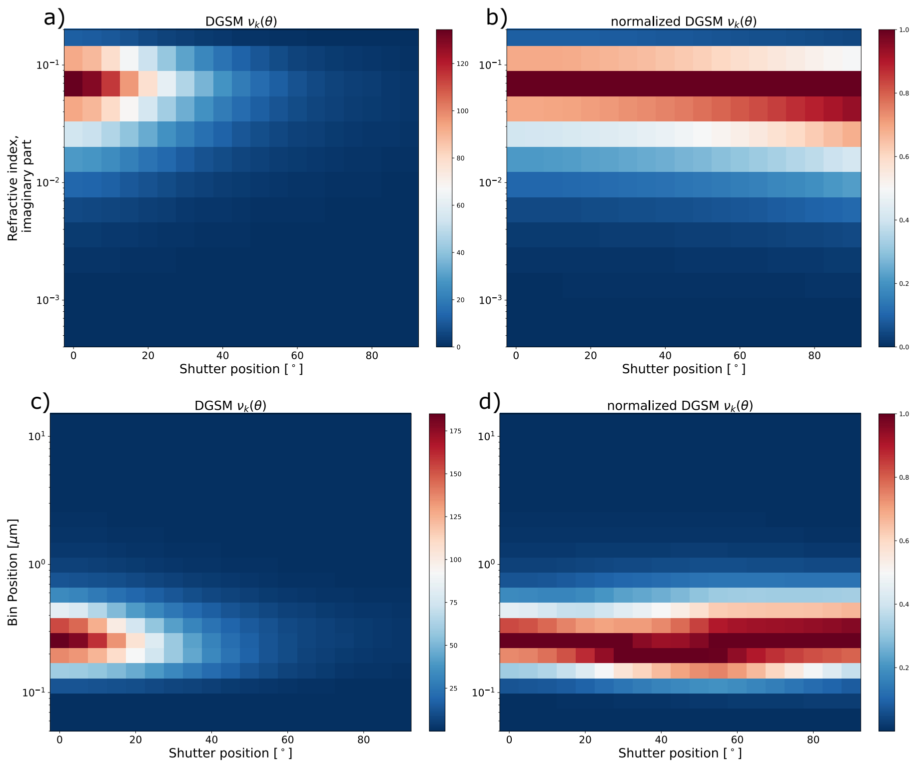

Figure 3. (a) $\nu_k(\theta)$ DGSM as a function of shutter and bin positions, and (b) $\nu_k(\theta)$ as a function of the imaginary part of the refractive index and bin position.

to fine-mode aerosol concentrations. In contrast, for particles with radii in the range of approximately 3–5 μm, the required concentration changes increase to values between 1 and 10 $\mu\text{m}^3\,\text{cm}^{-3}$. For larger particles, the required concentration changes exceed 10 $\mu\text{m}^3\,\text{cm}^{-3}$, reflecting the rapidly decreasing sensitivity of the nephelometer to coarse-mode aerosol perturbations. Only a weak dependence on wavelength is observed across the investigated size range. In contrast, the dependence on the absorbing component of the refractive index is more pronounced. For absorbing aerosols, the concentration thresholds corresponding to 1 and 10 $\mu\text{m}^3\,\text{cm}^{-3}$ shift toward smaller particle radii. As a result, for absorbing particles with radii exceeding approximately 1 μm, detectable signal changes already require concentration perturbations larger than 10 $\mu\text{m}^3\,\text{cm}^{-3}$. This behavior highlights the reduced sensitivity of the integrating nephelometer to coarse-mode absorbing aerosols and confirms that the measurable signal response is dominated by fine-mode particles.

These results confirm that the coarse aerosol mode is only weakly sensed by an integrating nephelometer and that the prospects for retrieving coarse-mode size-distribution parameters from nephelometer measurements are very limited under typical atmospheric conditions. To assess whether this conclusion is also quantitatively consistent, the detection thresholds derived above can be compared with realistic aerosol concentrations.

https://doi.org/10.5194/egusphere-2026-4754
Preprint. Discussion started: 10 August 2026

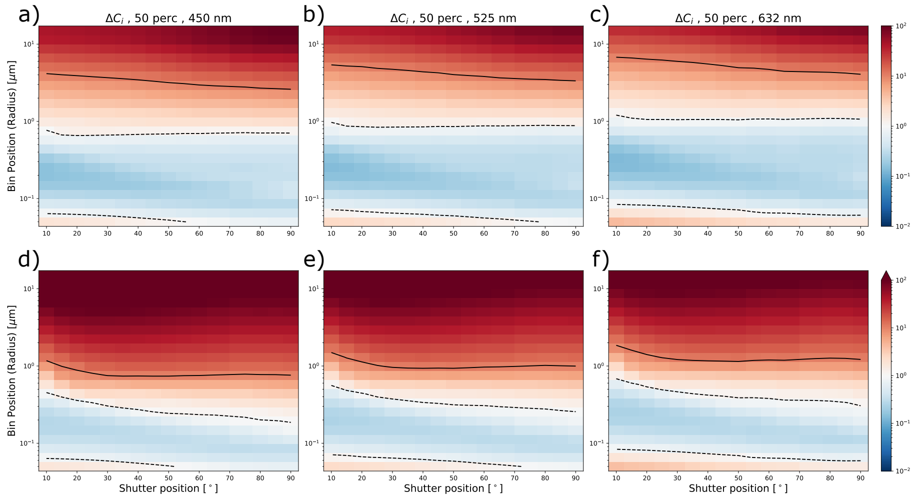

Figure 4. Change of i-th size bin concentration causing 3 % change of characteristic nephelometer signal measured at Raciborz. The solid and dashed contour lines depict values of 10 and 1, respectively.

As a representative example, we assume the typical PM_{10} concentration at the Racibórz observatory of approximately 20 μg m^{-3}. Under the simplifying assumption that this mass is equally partitioned between fine and coarse aerosol modes, the resulting coarse-mode mass concentration is about 10 μg m^{-3}. For a particle density of 1 g cm^{-3}, this corresponds to a total coarse-mode aerosol volume of approximately 10 μm^3 cm^{-3}.

The analysis presented in Fig. 4 shows that, for particles with radii larger than approximately 3–5 μm, concentration changes required to produce a detectable (3 %) variation in the nephelometer signal lie in the range of several to more than 10 μm^3 cm^{-3}. For even larger particles, the required concentration changes exceed 10 μm^3 cm^{-3}. Consequently, under realistic atmospheric conditions, the total single-bin coarse-mode concentration is of the same order as the minimum concentration change required to produce a measurable nephelometer response.

This implies that even large relative changes in the coarse-mode aerosol loading may result in only weak or marginally detectable changes in the nephelometer signal. As a result, the retrieval of detailed coarse-mode size-distribution parameters, such as individual bin concentrations or size characteristics, is generally not feasible in typical situations. This finding is fully consistent with the earlier GDSM sensitivity analysis and with the low degrees of freedom for signal derived for the integrating nephelometer.

Overall, this analysis demonstrates that the limited sensitivity to the coarse aerosol mode is not an artefact of the methodology, but rather a direct consequence of both the nephelometer measurement geometry and realistic atmospheric aerosol concentrations. Accordingly, the information provided by nephelometer measurements is dominated by fine-mode aerosol contributions, while the coarse mode remains largely unconstrained.

https://doi.org/10.5194/egusphere-2026-4754
Preprint. Discussion started: 10 August 2026

3.4 Information Content Analysis and Retrievable Moments of the Aerosol Size Distribution

The analysis presented above indicates that the coarse aerosol mode is nearly non-retrievable under realistic atmospheric conditions. This raises the question of how many independent moments of the aerosol size distribution can, in practice, be retrieved from integrating nephelometer measurements. To address this question, an information content analysis based on the foreward model's degrees of freedom for signal (DFS) is performed using singular value decomposition (SVD) of the Jacobian matrix.

The measured integrated scattering signal at shutter position θ_j is defined as

$$S_j = P_{\mathrm{int}}(\theta_j) = \sum_{i=1}^{22} c_i\,\Phi_i(\theta_j) = \sum_{i=1}^{22} c_i\,\Phi_{ij}, \tag{22}$$

where c_i denotes the concentration of the i-th aerosol size bin and $\Phi_i(\theta_j)$ represents its contribution to the integrated scattering signal at shutter position θ_j.

For the DFS analysis, the aerosol size distribution is parameterized in terms of a bimodal representation, with each mode described by a modal volume concentration, modal radius, and distribution width. The parameter vector is therefore defined as

$$\mathbf{p} = (\log N_f, \log R_f, \sigma_f, \log N_c, \log R_c, \sigma_c)\,, \tag{23}$$

where the subscripts f and c denote the fine and coarse modes, respectively.

The Jacobian matrix is constructed as the set of partial derivatives of the forward model with respect to the parameters $\mathbf{p}$, evaluated at a representative reference state $\mathbf{p}_0$,

$$J_{jk} = \left.\frac{\partial S_j}{\partial p_k}\right|_{\mathbf{p}_0}. \tag{24}$$

As the reference state $\mathbf{p}_0$, the median aerosol size distribution observed at the Racibórz station, measured using SMPS and APS instruments, is adopted.

The DFS analysis is carried out separately for three cases: the fine mode alone, the coarse mode alone, and the combined bimodal fine–coarse distribution. This separation allows a direct assessment of the independent information content associated with each aerosol mode and provides a quantitative measure of how many moments of the respective size distributions can be constrained by the integrating nephelometer measurements for different aerosol types, including non-absorbing continental sulfates, absorbing aerosols, and water-soluble marine-like particles.

The DFS analysis shows that, when the fine or coarse aerosol mode is considered individually, the degrees of freedom for signal are limited mainly to two. This indicates that not all parameters describing a single aerosol mode can be independently retrieved from integrating nephelometer measurements. In particular, strong parameter correlations prevent the simultaneous retrieval of modal concentration, modal radius, and distribution width. An exception is found for the fine absorbing aerosol case, for which a DFS value of three is obtained, indicating that all three fine-mode parameters can be constrained. This enhanced

https://doi.org/10.5194/egusphere-2026-4754
Preprint. Discussion started: 10 August 2026

Table 2. Degrees of freedom for signal (DFS) obtained from the SVD analysis for different aerosol types.

Aerosol type	**DFS (total)**	**DFS (fine)**	**DFS (coarse)**
Non-absorbing continental, $m = 1.48 + 0i$	3	2	2
Absorbing continental, $m = 1.48 + 0.5i$	3	3	2
Water soluble, $m = 1.36 + 0i$	3	2	2

retrievability is likely a consequence of the increased sensitivity of the forward model to absorbing aerosols, as previously demonstrated by the GDSM analysis.

For bimodal aerosol size distributions, consisting of both fine and coarse modes, the DFS is consistently limited to three for all investigated aerosol types defined as different refractive indexes. This result highlights the strong coupling between fine- and coarse-mode parameters introduced by the integrating nature of the nephelometer measurement. Rather than providing independent information on each mode separately, the measurements primarily constrain a limited number of combined moments of the full size distribution. As a consequence, only a small subset of distribution parameters can be retrieved simultaneously, while individual fine- and coarse-mode parameters remain strongly interdependent.

The correlation analysis of the Fisher information matrix (Appendix A, Tables A1–A3) provides a consistent interpretation of the DFS results and clarifies how the available information is distributed among aerosol parameters. While the total number of independent information channels is limited to DFS(total) = 3 for all investigated aerosol types, the correlation structure reveals strong parameter degeneracies that restrict which individual parameters can be robustly retrieved.

For non-absorbing continental and sea-salt-like aerosols, the correlation matrices are characterized by pronounced internal degeneracies within both aerosol modes. In the fine mode, modal concentration and distribution width are almost perfectly anti-correlated, indicating that these parameters cannot be independently constrained. Within the coarse mode, modal concentration, modal radius, and distribution width are all strongly correlated, demonstrating that the internal structure of the coarse mode is effectively unconstrained. In addition, strong inter-modal correlations indicate that fine and coarse contributions are tightly coupled through their shared influence on the total scattering signal. Consequently, the nephelometer primarily responds to overall scattering strength and to a limited contrast between aerosol modes, rather than to detailed microphysical structure. This behavior explains why the retrievable information remains restricted to three independent parameter combinations.

For absorbing continental aerosols, a redistribution of information within parameter space is observed. Although strong degeneracies among fine-mode parameters persist, the degeneracy within the coarse mode is partially reduced. This reduction allows an additional independent direction associated with coarse particles to be resolved, consistent with DFS(coarse) = 3. At the same time, inter-modal correlations are weaker than in the non-absorbing cases, indicating a partial separation between fine- and coarse-mode contributions. Importantly, absorption does not increase the total information content, which remains limited to DFS(total) = 3, but rather redistributes the available information from the fine mode toward the coarse mode. Physically, this reflects the size-dependent nature of absorption, which introduces additional contrast for larger particles and partially breaks the scattering-driven degeneracy that dominates non-absorbing aerosols.

https://doi.org/10.5194/egusphere-2026-4754
Preprint. Discussion started: 10 August 2026

3.5 Information-Based Ranking of Retrievable Aerosol Parameters

The information content analysis presented above allows for a quantitative identification of aerosol parameter combinations that are intrinsically supported by angularly resolved nephelometer measurements. This identification is based on the joint interpretation of derivative-based sensitivities, the effective rank of the forward operator (DFS = 3), and the correlation structure of the Fisher information matrix.

The Fisher-matrix correlations provide direct insight into parameter identifiability. Correlation coefficients close to ± 1 indicate that two parameters produce nearly identical variations in the measured signal and are therefore not independently retrievable. Conversely, deviations from unity indicate the presence of residual sensitivity to differences between parameters. In this way, the Fisher matrix reveals which parameter combinations correspond to independent information directions in measurement space.

Although aerosol size distributions are typically parameterized using multiple lognormal parameters for fine and coarse modes, the correlation structure demonstrates that many of these parameters are strongly coupled. Consequently, the measurements support only a limited number of independent parameter combinations, which can be ranked according to their stability and robustness.

3.5.1 Total aerosol concentration (highest importance).

$$N_{\text{tot}} = N_f + N_c \tag{25}$$

The total aerosol concentration corresponds to the dominant information direction. For all aerosol types considered, fine- and coarse-mode concentrations are strongly correlated (Tables A1–A3), indicating that their variations affect the measurements primarily through their combined contribution to the total scattering signal. While individual modal concentrations cannot be separated, their sum is robustly constrained and exhibits weaker effective coupling to other parameters. The total concentration therefore represents the least degenerate and most stable parameter combination and constitutes the primary output of nephelometer measurements.

3.5.2 Fine–coarse partitioning (secondary importance).

$$\eta_{f/c} = \frac{N_f}{N_f + N_c} \tag{26}$$

Although fine- and coarse-mode concentrations are strongly correlated, the correlation coefficients remain below unity (Tables A1–A3). This indicates that the measurements are not exclusively sensitive to their sum, but retain a limited sensitivity to their relative contributions. This residual sensitivity implies that, in addition to the dominant total concentration signal, there exists a weaker but distinguishable contrast between fine and coarse aerosol contributions. This contrast does not correspond to independent retrieval of modal concentrations, but rather to a second independent parameter combination describing their relative partitioning. Although this information is substantially weaker than that associated with the total concentration, it remains distinguishable and therefore constitutes a valid secondary degree of freedom.

https://doi.org/10.5194/egusphere-2026-4754
Preprint. Discussion started: 10 August 2026

3.5.3 Effective particle size (moderate importance).

The third retrievable parameter corresponds to a characteristic size metric, best interpreted as an effective radius:

$$R_{\text{eff}} = \frac{\int r^3 n(r)\,\mathrm{d}r}{\int r^2 n(r)\,\mathrm{d}r}. \tag{27}$$

The Fisher-matrix correlations reveal that size-related parameters within each mode are subject to strong degeneracies. For example, correlations such as $\rho(\log N_f, \sigma_f) \approx -1$ and $\rho(\log N_c, \sigma_c) \approx -1$ in Tables A1 and A3 indicate that variations in distribution width are largely compensated by changes in concentration. Similarly, correlations between modal radius and width remain very high across all aerosol types. These near-unity correlations indicate that individual size-distribution parameters do not correspond to independent information directions, but instead collapse into a single effective size-related degree of freedom. The measurement is therefore not sensitive to modal radius or width separately, but to a combined metric that reflects both the characteristic particle size and the spread of the distribution. In practice, this combined sensitivity is naturally represented by the effective radius R_{eff}.

3.5.4 Coarse-mode parameters (non-retrievable).

The correlation structure further shows that coarse-mode parameters are strongly coupled both among themselves and with parameters describing the fine mode and total concentration. Correlation coefficients involving coarse-mode variables frequently approach unity (Tables A1–A3), indicating that their effects on the measured signal are nearly indistinguishable from those of other parameters.

This interpretation is consistent with the DGSM analysis, which shows that the measured scattering signal is primarily governed by fine-mode aerosol contributions. As a result, variations in coarse-mode parameters produce comparatively weaker and less distinct signatures in the measurements.

Taken together, these results indicate that coarse-mode parameters do not define independent information directions. Instead, their influence is absorbed into dominant parameter combinations, primarily the total aerosol concentration and the effective size metric. This strong degeneracy implies that individual coarse-mode parameters cannot be reliably constrained from nephelometer measurements alone.

3.6 Selection of Informative Shutter Positions for Aerosol Discrimination

The purpose of this section is therefore to identify a reduced set of shutter positions that enables effective discrimination between different aerosol types. Rather than maximizing angular sampling density, the focus is on selecting shutter positions that exhibit complementary responses to changes in aerosol microphysical and optical properties, as identified by the sensitivity and information content analyses described in Sect. 3.4 and 3.2. Importantly, the degree of redundancy and similarity between shutter positions is not universal, but depends on aerosol type. Different aerosol classes may exhibit characteristic angular response patterns, resulting in aerosol-type-specific structures of inter-angle similarity, e.g., coarse aerosols favor forward

https://doi.org/10.5194/egusphere-2026-4754
Preprint. Discussion started: 10 August 2026

Table 3. Definition of representative aerosol types used in the analysis. The parameter ranges reflect typical variability of size-distribution parameters and refractive indices for fine- and coarse-mode aerosols.

Aerosol type	Mode	r_m [μm]	σ_g	n	k
Sulfate	Fine	0.07–0.15	1.5–1.7	1.44	0.0
Organic	Fine	0.10–0.20	1.6–1.8	1.5	0.001
Absorbing fine	Fine	0.06–0.10	1.5–1.9	1.6	0.1
Dust	Coarse	0.50–1.50	1.5–2.0	1.55	0.005
Marine	Coarse	0.30–1.00	1.7–1.9	1.52	0.0

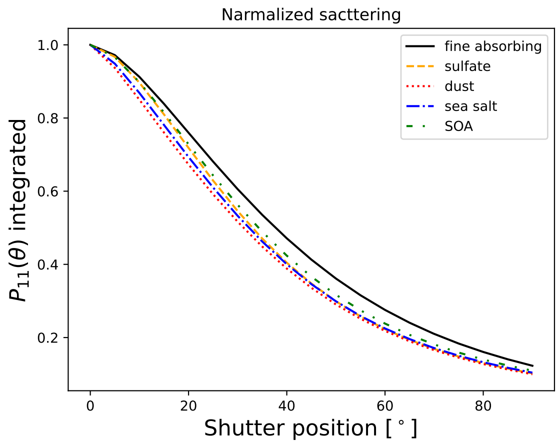

Figure 5. Normalized by total scattering nephelometer signal at 525 nm for each class of the aerosol.

scattering. This implies that the discriminative potential of individual shutter positions depends on the underlying aerosol properties rather than on instrument geometry alone.

The variance-ratio metric introduced in Sect. 2.4 was evaluated for a set of representative aerosol classes covering both fine-mode and coarse-mode dominated conditions. The aerosol definitions are summarized in Table 3. Angular scattering functions are calculated using mono-modal size distributions with systematic variability of the aerosol parameters. Subsequently, the variance within and between aerosol classes is evaluated for angularly dependent scattering signals normalized by the total scattering. An example of class-averaged normalized scattering functions is shown in Fig. 5. The absorbing aerosol class clearly deviates from the remaining aerosol types, exhibiting a distinct angular response. The analysis was performed at wavelengths of 450, 525, and 635 nm. Two scenarios were considered. In the first case, all aerosol classes listed in Table 3 were included. In the second case, the absorbing fine-mode aerosol class was excluded in order to isolate the influence of absorption. The resulting variance-ratio metric $D(\theta,\lambda)$ for all aerosol classes is presented in Fig. 6a, while the corresponding results obtained after excluding the absorbing aerosol class are shown in Fig. 6b. When all aerosol classes are considered, the variance-ratio metric exhibits a pronounced maximum near a shutter position of approximately 60° for all wavelengths. This maximum indicates that

https://doi.org/10.5194/egusphere-2026-4754
Preprint. Discussion started: 10 August 2026

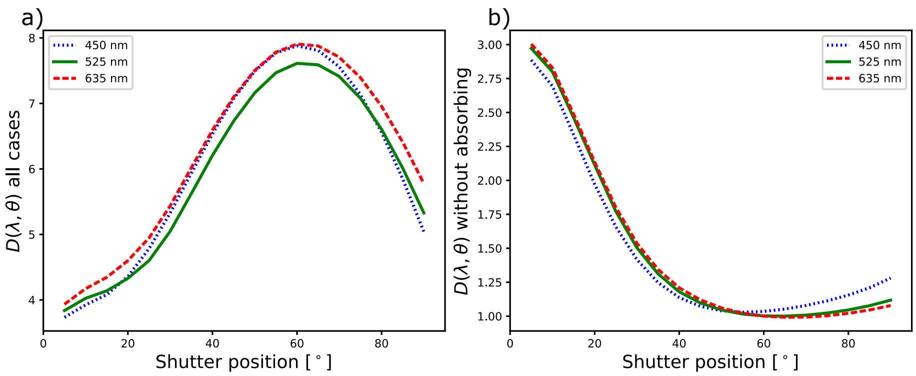

Figure 6. (a) Variance ratio for all cases, including absorbing aerosols. (b) Variance ratio excluding absorbing aerosols.

measurements performed at intermediate scattering angles provide the strongest separation between aerosol classes relative to their within-class variability. When the absorbing aerosol class is removed, the variance-ratio metric shows a local minimum in the same angular region. This behaviour demonstrates that the enhanced class separability near 60° is primarily associated with the presence of absorption. It indicates that, measurements in this angular range are particularly effective at distinguishing absorbing from non-absorbing aerosol types.

In contrast, discrimination among non-absorbing aerosol classes is achieved mainly through measurements at small scattering angles (below 20°) and large scattering angles (around 90°). These angular regions therefore contain complementary information on particle size and scattering regime. Consequently, an optimal angular sampling strategy should include both intermediate angles, which maximize sensitivity to absorption, and forward/backward scattering angles, which enhance discrimination among non-absorbing aerosol classes.

The observed behaviour is consistent with the theoretical framework introduced in Sect. 2.4. According to that framework, large values of $D(\theta, \lambda)$ indicate angular regions where the between-class variability dominates over the variability within individual aerosol classes. Such regions therefore provide the greatest potential for aerosol discrimination.

This is also consistent with the Fisher-information analysis presented above. Whereas the Fisher matrix quantifies parameter correlations and the number of independent information directions, the variance-ratio metric $D(\theta, \lambda)$ quantifies the separability of aerosol classes. Large values of $D(\theta, \lambda)$ correspond to angular regions where different aerosol classes produce distinct measurement signatures relative to their internal variability, while small values indicate a higher degree of overlap between classes. Therefore, the variance-ratio metric can be viewed as a class-based analogue of the Fisher-information analysis. The Fisher matrix identifies which combinations of aerosol parameters are potentially distinguishable, whereas $D(\theta, \lambda)$ identifies the angular regions in which these differences are most strongly expressed in measurement space. Consequently, maxima of $D(\theta, \lambda)$ indicate shutter positions expected to provide the strongest discrimination between competing aerosol models and the greatest potential contribution to aerosol classification and retrieval performance.

To better understand the angular dependence of the variance-ratio metric discussed in Sect. 2.4, Fig. 7 presents the distributions of the normalized nephelometer signal for individual aerosol classes at selected shutter positions. The violin plots provide

https://doi.org/10.5194/egusphere-2026-4754
Preprint. Discussion started: 10 August 2026

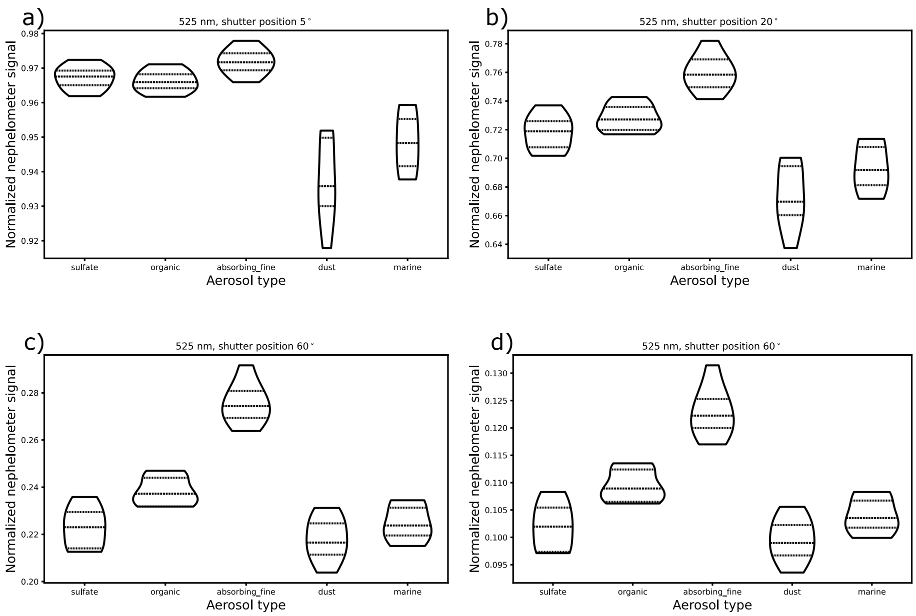

Figure 7. (a) total scattering, shutter position 5°. (b) shutter position 20°. (c) shutter position 60°. (d) backward scattering, shutter position 90°.

a direct visualization of both the mean class response and the within-class variability resulting from the range of particle-size distribution parameters used in Table 3.

For the smallest shutter positions (Figs. 7a and 7b), the normalized signal primarily reflects differences between fine-mode and coarse-mode dominated aerosols. In particular, marine and dust aerosols are clearly separated from sulfate, organic, and absorbing fine-mode aerosols. This behaviour is consistent with the strong influence of particle size on near-forward scattering and explains the enhanced discrimination between coarse and fine aerosol populations observed at small scattering angles.

At intermediate shutter positions (Fig. 7c), the separation between aerosol classes changes substantially. The absorbing fine-mode aerosol becomes distinctly separated from the remaining classes, while the overlap among non-absorbing aerosols increases. This behavior is consistent with the pronounced maximum of the variance-ratio metric near 60° shown in Fig. 6a and indicates that this angular region is particularly sensitive to aerosol absorption.

At larger shutter positions (Fig. 7d), the separation between the absorbing and non-absorbing aerosol classes decreases, while differences among non-absorbing aerosol types become more visible. Consequently, backward-scattering angles provide complementary information to that obtained from intermediate angles and contribute to the discrimination of aerosol classes that exhibit similar absorption properties but different particle-size distributions.

Taken together, Figs. 6 and 7 demonstrate that different angular regions emphasize different aspects of aerosol microphysics. Small scattering angles primarily separate coarse-mode and fine-mode aerosols, intermediate angles maximize sensitivity to absorption, and large scattering angles provide additional discrimination among non-absorbing aerosol classes. These results

https://doi.org/10.5194/egusphere-2026-4754
Preprint. Discussion started: 10 August 2026

explain the angular structure of the variance-ratio metric and provide physical insight into the selection of optimal shutter positions.

It should be noted that these results are obtained for an idealized case of mono-modal aerosol size distributions. For realistic atmospheric aerosols, which are typically characterized by bimodal size distributions, interactions between the fine and coarse modes are expected. Such interactions may reduce the clarity of separation between aerosol types and introduce additional complexity into aerosol classification based on angular scattering measurements.

4 Conclusions

In this study, the information content of angularly resolved nephelometer measurements was investigated using the GRASP forward model combined with derivative-based global sensitivity measures (DGSM), singular-value analysis, Fisher-information analysis, and an angular class-separability metric. The objective was to identify which aerosol properties are independently represented in the measured signal and to determine how the selection of angular sampling influences the information available from the instrument.

The DGSM analysis showed that nephelometer measurements are primarily sensitive to fine-mode aerosol properties and to strongly absorbing particles. In contrast, coarse-mode aerosol parameters generally exhibit considerably weaker sensitivity. This behaviour is consistent with the results obtained from the singular-value decomposition and Fisher-matrix analysis, which indicate that only a limited number of independent parameter combinations are effectively represented in the measurements. For the representative aerosol populations considered in this study, the effective dimensionality of the measurement space is approximately three. Although aerosol size distributions are commonly described using several lognormal parameters, most of these parameters are strongly coupled and do not correspond to independent information directions. The analysis suggests that the three dominant independent aerosol properties are, in decreasing order of importance,

$$N_{\text{tot}} \to \eta_{f/c} \to R_{\text{eff}}, \tag{28}$$

where N_{tot} denotes the total aerosol concentration, $\eta_{f/c}$ describes the fine-to-coarse partitioning, and R_{eff} represents an effective size parameter that combines information on both characteristic particle size and distribution width.

The strong parameter correlations revealed by the Fisher matrix show that many aerosol size-distribution parameters are effectively interchangeable and provide redundant information. Particularly strong overlaps are found among coarse-mode parameters, whose influence is largely absorbed into the dominant concentration and size-related information directions. As a result, the measurements are primarily sensitive to fine-mode concentration and size characteristics, whereas only relatively large perturbations of coarse-mode properties lead to clearly detectable changes in the signal.

The singular-value and Fisher analyses further demonstrate that increasing the number of measured angular channels does not increase the number of independent degrees of freedom available in the observations. The redundancy originates from the physical structure of the scattering operator itself rather than from any specific retrieval methodology. Consequently, dense angular sampling provides multiple measurements of the same information directions rather than generating new independent

https://doi.org/10.5194/egusphere-2026-4754
Preprint. Discussion started: 10 August 2026

information. The analysis of the variance-ratio metric confirms this conclusion and provides a practical framework for selecting angular sampling positions. Because neighboring shutter positions often contain highly redundant information for a given aerosol type, the optimal strategy is not to sample as many angles as possible, but to select a limited set of angles that maximize discrimination between different aerosol classes. The results show that different angular regions emphasize different aspects of aerosol microphysics. Small scattering angles, including the total-scattering measurement and angles below approximately 20°, provide the best separation between fine-mode and coarse-mode aerosol populations. Intermediate angles around 60° are particularly effective for identifying absorbing aerosol components, while large scattering angles in the backscattering region (90°–170°) provide complementary information useful for distinguishing non-absorbing aerosol classes.

Based on the combined DGSM, Fisher, SVD, and angular-separability analyses, we recommend a reduced measurement configuration consisting of four angular positions: total scattering, approximately 20°, approximately 60°, and one representative backscattering angle near 90°. This number exceeds the estimated DFS of three, providing a desirable level of measurement redundancy while retaining the principal information content of the full angular scan. Such a configuration would allow improved signal-to-noise performance through increased averaging at individual angles while significantly reducing redundancy in angular sampling.

Finally, the results highlight the importance of using aerosol parameterizations that are consistent with the intrinsic information content of nephelometer observations. Since only three independent aerosol properties are supported by the measurements, overly complex aerosol models may introduce strong parameter compensation effects, whereby changes in one parameter are balanced by changes in another without producing distinct changes in the measured signal. Future analyses and retrieval frameworks should therefore strive to match model complexity to the effective dimensionality of the measurement space identified in this study.

Code and data availability. GRASP-OPEN version 1.1.6 used in this study is publicly available at https://www.grasp-open.com. The numerical outputs used for the information-content analyses are available from the corresponding author upon reasonable request in NetCDF format.

Appendix A: Fisher Matrix Correlation Analysis

This appendix presents the correlation matrices of the Fisher information matrix for the different aerosol types considered in this study. The matrices illustrate the degree of parameter degeneracy within and between the fine and coarse aerosol modes and support the interpretation of the DFS results discussed in the main text.

Author contributions. AP: Conceptualization, Methodology, Software, Formal analysis, Validation, Visualization, Writing, Resources. IB: Conceptualization, Validation, Writing. AS: Methodology, Validation, Visualization, Writing. JS: Software, Writing.

https://doi.org/10.5194/egusphere-2026-4754
Preprint. Discussion started: 10 August 2026

Table A1. Correlation matrix of the Fisher information matrix for non-absorbing continental (sulfate) aerosol.

	$\log N_f$	$\log R_f$	σ_f	$\log N_c$	$\log R_c$	σ_c
$\log N_f$	1.000	0.819	-1.000	0.953	-0.954	-0.949
$\log R_f$	0.819	1.000	-0.814	0.923	-0.920	-0.921
σ_f	-1.000	-0.814	1.000	-0.949	0.950	0.946
$\log N_c$	0.953	0.923	-0.949	1.000	-0.995	-1.000
$\log R_c$	-0.954	-0.920	0.950	-0.995	1.000	0.993
σ_c	-0.949	-0.921	0.946	-1.000	0.993	1.000

Table A2. Correlation matrix of the Fisher information matrix for absorbing continental aerosol.

	$\log N_f$	$\log R_f$	σ_f	$\log N_c$	$\log R_c$	σ_c
$\log N_f$	1.000	0.025	-1.000	0.821	-0.887	-0.777
$\log R_f$	0.025	1.000	-0.024	0.432	-0.428	-0.435
σ_f	-1.000	-0.024	1.000	-0.817	0.884	0.773
$\log N_c$	0.821	0.432	-0.817	1.000	-0.964	-0.996
$\log R_c$	-0.887	-0.428	0.884	-0.964	1.000	0.937
σ_c	-0.777	-0.435	0.773	-0.996	0.937	1.000

Table A3. Correlation matrix of the Fisher information matrix for sea-salt-like aerosol.

	$\log N_f$	$\log R_f$	σ_f	$\log N_c$	$\log R_c$	σ_c
$\log N_f$	1.000	0.891	-1.000	0.946	-0.950	-0.941
$\log R_f$	0.891	1.000	-0.885	0.954	-0.955	-0.949
σ_f	-1.000	-0.885	1.000	-0.940	0.945	0.936
$\log N_c$	0.946	0.954	-0.940	1.000	-0.996	-1.000
$\log R_c$	-0.950	-0.955	0.945	-0.996	1.000	0.994
σ_c	-0.941	-0.949	0.936	-1.000	0.994	1.000

https://doi.org/10.5194/egusphere-2026-4754
Preprint. Discussion started: 10 August 2026

Acknowledgements. The authors gratefully acknowledge the GRASP development team for their invaluable support and for providing the open-source Generalized Retrieval of Aerosol and Surface Properties (GRASP) code. The source code and documentation are publicly available at https://www.grasp-open.com.

https://doi.org/10.5194/egusphere-2026-4754
Preprint. Discussion started: 10 August 2026

References

Anderson, T. L. and Ogren, J. A.: Determining aerosol radiative properties using the TSI 3563 integrating nephelometer, Aerosol Science and Technology, 29, 57–69, https://doi.org/10.1080/02786829808965551, 1998.

Anderson, T. L., Covert, D. S., Wheeler, J. D., Harris, J. M., and Perry, K. D.: Performance characteristics of a high-sensitivity, three-wavelength, total scatter/backscatter nephelometer, Journal of Atmospheric and Oceanic Technology, 13, 967–986, 1996.

Bazo, E., Martins, J., Perez-Ramirez, D., Valenzuela, A., Titos, G., Cazorla, A., Fuertes, D., Weiss, M., Turpie, A., Li, C., García-Izquierdo, F., Foyo-Moreno, I., Alados-Arboledas, L., and Olmo, F.: Optimization of the Polarized Imaging Nephelometer (PI-Neph) for continuous monitoring of multiwavelength aerosol phase functions in support of space polarimetry missions, Atmospheric Environment, 316, 120 181, https://doi.org/10.1080/02786820903156542, 2024.

Beuttell, R. G. and Brewer, A. W.: Instruments for the Measurement of the Visual Range, Journal of Scientific Instruments, 26, 357–359, https://doi.org/10.1088/0950-7671/26/11/302, 1949.

Chamberlain-Ward, S. and Sharp, F.: Advances in nephelometry through the Ecotech Aurora nephelometer, The Scientific World Journal, 11, 2530–2535, https://doi.org/10.1100/2011/310769, 2011.

Dubovik, O. and King, M. D.: A flexible inversion algorithm for retrieval of aerosol optical properties from Sun and sky radiance measurements, Journal of Geophysical Research: Atmospheres, 105, 20 673–20 696, 2000.

Dubovik, O., Sinyuk, A., Lapyonok, T., Holben, B. N., Mishchenko, M., Yang, P., Eck, T. F., Volten, H., Muñoz, O., Veihelmann, B., et al.: Application of spheroid models to account for aerosol particle nonsphericity in remote sensing of desert dust, Journal of Geophysical Research: Atmospheres, 111, 2006.

Dubovik, O., Herman, M., Holdak, A., Lapyonok, T., Tanré, D., Deuzé, J.-L., Ducos, F., Sinyuk, A., and Lopatin, A.: Statistically optimized inversion algorithm for enhanced retrieval of aerosol properties from spectral multi-angle polarimetric satellite observations, Atmospheric Measurement Techniques, 4, 975–1018, https://doi.org/10.5194/amt-4-975-2011, 2011.

Dubovik, O., Lapyonok, T., Litvinov, P., Herman, M., Fuertes, D., et al.: GRASP: a versatile algorithm for characterizing the atmosphere, SPIE Newsroom, https://doi.org/10.1117/2.1201408.005558, 2014.

Dubovik, O., Fuertes, D., Litvinov, P., Lopatin, A., Lapyonok, T., et al.: A Comprehensive Description of Multi-Term LSM for Applying Multiple a Priori Constraints in Problems of Atmospheric Remote Sensing: GRASP Algorithm, Concept, and Applications, Frontiers in Remote Sensing, 2, 706 851, https://doi.org/10.3389/frsen.2021.706851, 2021.

Engl, H. W., Hanke, M., and Neubauer, A.: Regularization of Inverse Problems, Springer, Dordrecht, https://doi.org/10.1007/978-94-009-1740-8, 1996.

Espinosa, W. R., Remer, L. A., Dubovik, O., Ziemba, L., and Beyersdorf, A.: Retrievals of aerosol optical and microphysical properties from imaging polar nephelometer scattering measurements, Atmospheric Measurement Techniques, 10, 811–824, https://doi.org/10.5194/amt-10-811-2017, 2017.

Hansen, P. C.: Rank-Deficient and Discrete Ill-Posed Problems: Numerical Aspects of Linear Inversion, SIAM, Philadelphia, https://doi.org/10.1137/1.9780898719697, 1998.

Horvath, H. and Kaller, W.: Calibration of integrating nephelometers in the post-halocarbon era, Atmospheric Environment, 28, 1219–1223, https://doi.org/10.1016/1352-2310(94)90299-2, 1993.

Iooss, B., Lemaître, P., et al.: A review on global sensitivity analysis methods, Reliability Engineering & System Safety, 94, 667–679, https://doi.org/10.1016/j.ress.2008.04.007, 2010.

https://doi.org/10.5194/egusphere-2026-4754
Preprint. Discussion started: 10 August 2026

Kress, R.: Linear Integral Equations, Springer, New York, 2 edn., https://doi.org/10.1007/978-1-4612-0559-3, 1999.

Laj, P. et al.: The ACTRIS research infrastructure: Long-term aerosol, cloud, and trace gas observations for atmospheric science, Bulletin of the American Meteorological Society, 105, E536–E558, https://doi.org/10.1175/BAMS-D-23-0021.1, 2024.

Lopatin, A., Dubovik, O., Chaikovsky, A., Goloub, P., Lapyonok, T., Tanré, D., Litvinov, P., and Herman, M.: Enhancement of aerosol characterization using synergy of lidar and sun-photometer coincident observations: the GARRLiC algorithm, Atmospheric Measurement Techniques, 6, 2065–2088, https://doi.org/10.5194/amt-6-2065-2013, 2013.

Lopatin, A., Dubovik, O., Fuertes, D., Stenchikov, G., Lapyonok, T., Veselovskii, I., Wienhold, F. G., Shevchenko, I., Hu, Q., and Parajuli, S.: Synergy processing of diverse ground-based remote sensing and in situ data using the GRASP algorithm: applications to radiometer, lidar and radiosonde observations, Atmospheric Measurement Techniques, 14, 2575–2614, https://doi.org/10.5194/amt-14-2575-2021, 2021.

Massoli, P., Murphy, D. M., Lack, D. A., Baynard, T., Brock, C. A., and Lovejoy, E. R.: Uncertainty in Light Scattering Measurements by TSI Nephelometer: Results from Laboratory Studies and Implications for Ambient Measurements, Aerosol Science and Technology, 43, 1064–1074, https://doi.org/10.1080/02786820903156542, 2009.

Michibata, T., Wall, C., Hirota, N., Duran, B., and Nozawa, T.: Recent Advances in the Observation and Modeling of Aerosol-Cloud Interactions, Cloud Feedbacks, and Earth's Energy Imbalance: A Review, Current Pollution Reports, 11, 1–18, https://doi.org/10.1007/s40726-025-00382-6, 2025.

Moallemi, A., Modini, R. L., Lapyonok, T., Lopatin, A., Fuertes, D., Dubovik, O., Giaccari, P., and Gysel-Beer, M.: Information content and aerosol property retrieval potential for different types of in situ polar nephelometer data, Atmospheric Measurement Techniques, 15, 5619–5642, https://doi.org/10.5194/amt-15-5619-2022, 2022.

Müller, T., Laborde, M., Kassell, G., and Wiedensohler, A.: Design and performance of a three-wavelength LED-based total scatter and backscatter integrating nephelometer, Atmospheric Measurement Techniques, 4, 1291–1303, https://doi.org/10.5194/amt-4-1291-2011, 2011.

Regayre, L. A., Prévost, L. M. C., Ghosh, K., Johnson, J. S., Oakley, J. E., Owen, J., Webb, I., and Carslaw, K. S.: Remaining aerosol forcing uncertainty after observational constraint and the processes that cause it, Atmospheric Chemistry and Physics, 26, 2293–2317, https://doi.org/10.5194/acp-26-2293-2026, 2026.

Rodgers, C. D.: Inverse Methods for Atmospheric Sounding: Theory and Practice, World Scientific, Singapore, https://doi.org/10.1142/3171, 2000.

Sobol, I. M.: Global sensitivity indices for nonlinear mathematical models and their Monte Carlo estimates, Mathematics and Computers in Simulation, 55, 271–280, https://doi.org/10.1016/S0378-4754(00)00270-6, 2001.

Sobol, I. M. and Kucherenko, S.: Derivative based global sensitivity measures and their link with global sensitivity indices, Mathematics and Computers in Simulation, 79, 3009–3017, https://doi.org/10.1016/j.matcom.2009.01.023, 2009.